Research Article

pISSN 1225-6161 • eISSN 2287-9307
Korean Journal of Remote Sensing 2025, 41(5), 843-857
https://doi.org/10.7780/kjrs.2025.41.5.11

Korean Journal of Remote Sensing
KJRS

Impact of Urban Tree Canopy on Land Surface Temperature and Green Space Inequities in Suwon, South Korea

Yeonsu Lee[1], Sun Jegal[2], Siwoo Lee[1], Bokyung Son[1], Jungho Im[3]*

[1]Combined MS/PhD Student, Department of Civil Urban Earth and Environmental Engineering, Ulsan National Institute of Science and Technology, Ulsan, Republic of Korea
[2]Undergraduate Student, Department of Civil Urban Earth and Environmental Engineering, Ulsan National Institute of Science and Technology, Ulsan, Republic of Korea
[3]Professor, Department of Civil Urban Earth and Environmental Engineering, Ulsan National Institute of Science and Technology, Ulsan, Republic of Korea

Abstract: Urban trees provide benefits that reduce urban heat stress, but these benefits are often inequitably distributed. Most existing research relies on coarse-resolution data that fail to capture fine-scale spatial distributions of green space and the associated social inequalities. This study addresses that critical gap by investigating vegetation-heat dynamics and environmental equity in a dense urban environment. To achieve a high-resolution analysis, we examined Suwon, South Korea, by integrating a 0.25 m tree canopy map with 30 m Landsat 8-derived land surface temperature (LST), key socioeconomic indicators, and the local climate zone (LCZ) framework. We quantified the seasonal relationship between total green space (TGS) and LST, assessed fraction-dependent cooling effects, assessed green space per capita, and identified administrative districts where vegetation is scarce, heat exposure is extreme, and the elderly population is high. Our results revealed a significant, nonlinear cooling effect: the thermal benefits of tree canopy increase sharply up to approximately 40% coverage before diminishing. The key finding is the confirmation of severe spatial inequality of TGS. Dense urban cores, which have high concentrations of vulnerable elderly residents, frequently fall below the World Health Organization's 9 m^2 greenspace per person standard. In contrast, peripheral neighborhoods retain extensive forest canopy, highlighting a systemic disparity in access to green infrastructure. This study provides one of the first fine-scale assessments of vegetation–heat equity in a Korean city. By linking fraction-dependent cooling with spatial inequities, it demonstrates the need for targeted greening strategies that advance both climate adaptation and environmental justice.

Keywords: Greenspace inequity, Heat mitigation, Heat vulnerability, Land surface temperature, Tree canopy cover, Local climate zone, Fraction-dependent cooling

Received: September 30, 2025
Revised: October 21, 2025
Accepted: October 25, 2025
Published: October 31, 2025

Corresponding author:
Jungho Im
E-mail: ersgis@unist.ac.kr

1. Introduction

Rapid urbanization has intensified thermal stress in cities, and heat waves are increasingly recognized as a critical public health and environmental challenge (Koppe et al., 2004; Gao et al., 2024). Because the elderly population is particularly vulnerable to heat stress, reducing urban heat exposure is a top priority for climate adaptation and sustainable urban planning (Falchetta et al., 2024; Somvanshi et al., 2025).

Urban trees are among the most effective and multifunctional forms of green infrastructure (Alonzo et al., 2025; Yin et al., 2024). Through shading and evapotranspiration, trees mitigate urban heat islands (Wang et al., 2023; Zhan et al., 2024), reduce air pollution (Kofel et al., 2024), and improve human thermal comfort (Gillerot et al., 2024), while also contributing to biodiversity and overall quality of life (Lee et al., 2024; Wu et al., 2024). However,

the benefits of urban trees are not equitably distributed across all neighborhoods. Previous studies have repeatedly shown that wealthier areas tend to enjoy greater canopy cover, while socially disadvantaged communities often suffer from limited access to vegetation and disproportionate exposure to environmental risks (Heo et al., 2021; Li and Li, 2025). This imbalance reflects not only ecological disparities but also issues of environmental justice (Derickson et al., 2024).

Most existing research has analyzed the cooling benefits of vegetation using medium–resolution satellite-derived vegetation indices such as the normalized difference vegetation index (NDVI) or the enhanced vegetation index (EVI) (Xie et al., 2018; Du et al., 2022; Liu et al., 2024; Na et al., 2024). While these datasets are valuable for capturing city-wide patterns, they often fail to resolve fine-scale inequalities at the neighborhood or block level. In the North American cities, the National Land Cover Database (NLCD) tree canopy product has also been widely used to examine vegetation–temperature relationships (Jung et al., 2021; Zhou et al., 2021). However, NLCD systematically underestimates urban tree canopy, particularly in dense city environments where small, fragmented tree stands are common and often go undetected (Pourpeikari Heris et al., 2022).

To address these gaps, this study integrates a high-resolution (0.25 m) tree canopy map with Landsat-8–derived land surface temperature (LST), socioeconomic data, and the local climate zone (LCZ) framework to examine both the thermal and equity dimensions of urban vegetation in Suwon, South Korea. Our objectives of this study are 1) to assess how total green space (TGS) fractions influence LST across seasons; 2) to evaluate fraction-dependent cooling effects within different LCZ classes; 3) diagnose spatial inequities in green space distribution relative to population density and elderly residents; and 4) identify neighborhoods where vegetation scarcity, high heat exposure, and vulnerable populations converge. By linking the cooling role of vegetation with distributional equity, this study provides one of the first fine-scale assessments of tree-heat relationships in a Korean city. The findings generate an evidence base for targeted greening strategies that advance both climate adaptation and social equity.

2. Materials and Methods

2.1. Study Area

The study was conducted in Suwon, South Korea, a city of about 1.2 million residents (Fig. 1a). Suwon is characterized by a heterogeneous urban fabric that combines traditional low-rise residential neighborhoods with dense commercial cores and large-scale apartment complexes. The city is bordered by forested hills, producing sharp contrasts between built-up zones and natural areas. Suwon is administratively divided into 44 districts (dong), each exhibiting distinct socioeconomic characteristics. Newly developed high-rise residential clusters in southern and eastern districts—such as Gwanggyo (Gwanggyo 1(il)–dong and 2(i)–dong) and Yeongtong (Yeongtong 1(il)–dong to 3(sam)–dong)—are notable for their higher household incomes, younger populations, and planned green infrastructure. In contrast, o lder central neighborhoods like Ji–dong and Haenggung–dong are characterized by an elderly population, lower consumption capacity, and limited green spaces. This diversity of urban forms, socioeconomic contexts, and environmental settings makes Suwon an ideal case for examining vegetation distribution, its cooling effects on LST, and spatial inequities in access to green space across neighborhoods.

2.2. Data

2.2.1. High-Resolution Land Cover Map

We used a high-resolution (0.25 m) land-cover dataset for Suwon produced by Son et al. (2021). The dataset was generated by integrating airborne LiDAR data (height and intensity) acquired on September 27–28, 2020, and RGB orthophotos through a U-Net deep learning classification workflow. Validation against manually delineated tree reference data—constructed by digitizing tree crowns from LiDAR and supplementing with forest layers from the Ministry of Environment land-cover map—confirmed high classification accuracy (overall accuracy ≈ 92 %, tree class accuracy > 90 %). The product provides per-pixel classifications for tree, shrub, grass, cropland, wetland, vinyl greenhouse, bare land, water, building, and other impervious covers (Fig. 1b).

2.2.2. Local Climate Zone

To control the influence of urban morphology, we employed an LCZ classification framework (Stewart and Oke, 2012). The LCZ framework defines seventeen classes: ten urban types (LCZ 1–10) and seven natural types (LCZ A–G), reflecting differences in built form, surface cover, and thermal properties. For Suwon, we used the 2021 LCZ map developed by Lee et al. (2023b) using a convolutional neural network approach trained on Landsat and Sentinel imagery. The map has a spatial resolution of 30 m and reported accuracies of 91.10% overall, 81.27% for urban LCZ types, and 96.35% for natural LCZ types (Fig. 1c).

https://doi.org/10.7780/kjrs.2025.41.5.11

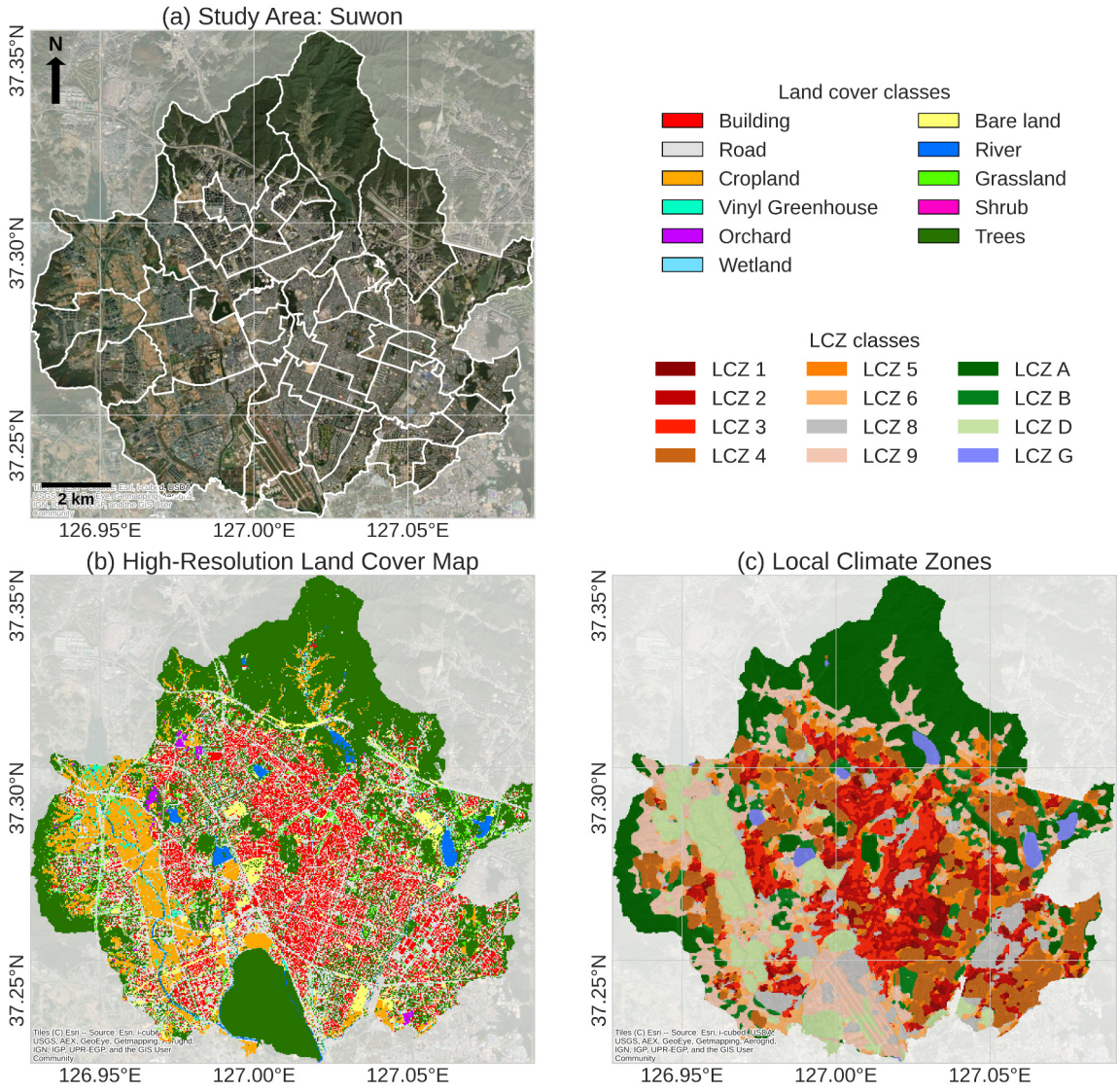

Fig. 1. Study area and input datasets for Suwon, South Korea. (a) Study area boundaries and administrative districts (44 dongs) overlaid on high-resolution satellite imagery. (b) High-resolution land cover map (0.25 m) from Son et al. (2021), with tree canopy, built-up, and other land-cover classes. (c) Local climate zone (LCZ) map made in Lee et al. (2023b) following Stewart and Oke (2012).

The use of LCZs in this study is critical for two reasons. First, it enables a clear distinction between built-up urban areas and natural landscapes within the city boundary, providing a robust baseline for comparison (Yoo et al., 2020). Second, the LCZ framework clusters areas with similar compositions and proportions of buildings and vegetation into homogeneous units. By analyzing relationships between vegetation and LST within these contextually consistent clusters, we can more accurately assess the cooling effects of vegetation, minimizing confounding influences from mixed urban forms and enabling a robust examination of vegetation-LST interactions across diverse urban settings.

2.2.3. Landsat 8 Collection 2 Data

To characterize thermal environments, we used Landsat 8 Collection 2 Level 1 (L1) and Level 2 (L2) data. Landsat 8 carries the Operational Land Imager (OLI) and the Thermal Infrared Sensor (TIRS). OLI provides multispectral data at 30 m resolution across the visible to shortwave infrared spectrum, while TIRS acquires thermal infrared data at a native spatial resolution of 100 m (Band 10: 10.6–11.2 μm; Band 11: 11.5–12.5 μm). The United States Geological Survey (USGS) distributes the Landsat 8 Collection 2 L1 and L2 products at 30 m spatial resolution using cubic-convolution resampling to co-register the TIRS bands with the 30 m OLI bands (United States Geological Survey, 2025a).

Due to known calibration issues in Band 11 (Jeevalakshmi et al., 2017), the official L2 Surface Temperature (ST) product used only Band 10 for temperature retrievals (Crawford et al., 2023).

Although the official L2 ST product was initially considered, it exhibited persistent, spatially systematic missing values across Suwon for every available clear-sky scene, particularly over the northern and high-elevation districts (Supplementary Fig. 1). According to the USGS Landsat Collection 2 Known Issues documentation (United States Geological Survey, 2025b), these missing values might result from missing or invalid emissivity inputs in the Advanced Spaceborne Thermal Emission and Reflection Radiometer (ASTER) Global Emissivity Dataset (GED), which is required for L2 ST generation. While we did not directly examine the ASTER GED inputs, the consistent pattern of these gaps across all dates suggests a structural rather than scene-specific issue, leading to discontinuous city-wide temperature fields. A similar issue was also reported by Lee et al. (2021), who analyzed the Landsat 8 Collection 2 L2 ST product in Suwon and Daegu from 2013 to 2021 and confirmed that the data gaps persisted over time. To address the missing data limitation and ensure spatial completeness, we independently derived LST from the L1 Band 10 radiance, as described in Section 2.3.1.

2.2.4. Socioeconomic Data

Socioeconomic indicators were obtained from the 2021 Suwon Statistical Yearbook. Variables included total population, population density, and the proportion of elderly residents aged 65 and above. These attributes were compiled at the dong level and used to assess disparities in green-space provision (e.g., per-capita green space) and related exposure across neighborhoods.

2.3. Methods

Our analysis grid was defined at a 30 m resolution, as this scale matches the resolution of the Landsat-derived LST and LCZ products, ensuring spatial consistency across all datasets. At this scale, the spatial heterogeneity and functional composition of cities can be effectively captured for urban thermal analysis (Yin et al., 2022; Shi et al., 2023). Thus, adopting a 30 m grid provides a coherent spatial framework for linking thermal, spectral, and morphological variables in city-scale assessments.

The primary study period was set to 2020, corresponding to the acquisition period of the high-resolution (0.25 m) land cover dataset. However, obtaining cloud-free Landsat 8 imagery during the humid Korean summer is extremely challenging. To secure sufficient clear-sky observations, we therefore extended the analysis period by one year before and after, incorporating all available cloud-free scenes from 2019 to 2021.

Kim and Kang (2022) reported that the city's total tree-canopy area changed by about 2 % over an entire decade (2003–2012), while the Suwon Council for Sustainable Development (2021) shows that the proportion of natural areas changed by only about 1.3% between 2012 and 2019. Based on this evidence, we assumed temporal stability in canopy distribution across the 2019–2021 period when analyzing vegetation-temperature relationships.

2.3.1. Preprocessing and Aggregation

We derived LST from Landsat 8 Collection 2 L1 TIRS Band 10 radiance using the single-channel algorithm (Sobrino et al., 2004). Surface emissivity (ε) was estimated from NDVI-derived vegetation proportion P_v as Eq. (1):

$$P_v = \left(\frac{(NDVI - NDVI_{min})}{(NDVI_{max} - NDVI_{min})}\right)^2, \varepsilon = 0.004\, P_v + 0.986 \quad (1)$$

LST was then obtained from Band-10 brightness temperature $BT(k)$ as Eq. (2):

$$LST = \frac{BT}{1 + \left(\frac{\lambda\, BT}{\rho}\right)\ln(\varepsilon)} \quad (2)$$

where λ denotes the central wavelength of Band 10 and ρ is a constant $h \times c / \sigma$ (1.438×10^{-2} mK). Here, h is Planck's constant (6.626×10^{-34}), c is the speed of light (3×10^8 m/s), and σ is the Boltzmann constant (1.38×10^{-23} J/K). This approach follows the same physical basis as the USGS Landsat L2 ST workflow (Crawford et al., 2023) and is widely applied in previous studies (Valor and Caselles, 1996; Guo et al., 2020; Chakraborty et al., 2021; Lee et al., 2023a).

To evaluate the accuracy, our retrievals were compared with Landsat 8 L2 ST (15 scenes; Supplementary Table 1) and in-situ LST from the Korea Meteorological Administration Automated Synoptic Observing System Suwon station (Supplementary Table 2). Finally, seasonal LST composites were produced by averaging all valid, cloud-free pixels for each season—spring (March–April–May), summer (June–July–August), fall (September–October–November), and winter (December–January–February). This multi-date scene compositing strategy minimizes day-specific biases caused by transient atmospheric and surface conditions (Sun et al., 2024), providing a more robust representation of seasonal thermal environments (Supplementary Table 3).

The 0.25 m land cover dataset was aggregated to the same 30

https://doi.org/10.7780/kjrs.2025.41.5.11

m grid as the LST and LCZ products. Within each grid cell, the fractional coverage of forest canopy (FC), urban tree canopy (UTC), and grass was calculated and combined to derive the TGS fraction. Here, FC refers to tree pixels located within natural LCZ types (A–G), corresponding to continuous forests, forested hillsides, and large urban parks. UTC refers to tree pixels located within urban LCZ types (1–10), corresponding to vegetation embedded in built-up areas such as street trees, residential courtyards, school yards, and small urban parks. The resulting 30 m green-space fractions were subsequently aggregated to the administrative dong level.

2.3.2. Analysis Overview

Our analytical framework comprised four components. First, at the pixel level, we evaluated the relationship between TGS and LST by grouping all 30 m grid cells into 5% TGS intervals and summarizing LST distributions by their median and interquartile range. Comparisons were made between urban LCZs (Classes 1–9) and natural LCZs (Classes A–G) to examine differences in vegetation–temperature relationships across built and natural contexts. Second, to investigate morphology-dependent cooling, we stratified the analysis by LCZ class and examined how LST distributions shifted across TGS fraction groups (0–20%, 20–40%, 40–60%, and 60–80%). Seasonal median LSTs were summarized by LCZ and TGS categories to reveal how vegetation effects varied across different urban forms.

Third, at the neighborhood (dong) scale, we quantified the composition of FC and UTC within each administrative unit, assessed spatial gradients in TGS, and related these to population density, greenspace per capita, and elderly population share. This enabled us to identify districts with especially limited vegetation relative to their demographic characteristics. Finally, we constructed a composite vulnerability index to integrate ecological scarcity, demographic sensitivity, and heat exposure. Vulnerability was defined using three internationally recognized criteria: (i) greenspace per capita below the World Health Organization (WHO) minimum standard of 9 m^2 per person (Kuchelmeister, 1998), (ii) elderly population share exceeding United Nations thresholds for aged (≥14%) or super-aged (≥20%) societies (Independent Evaluation Group, 2019), and (iii) summer mean LST values within the upper quartile of the citywide distribution. Districts satisfying one, two, or all three criteria were assigned scores of 1 (moderate), 2 (high), or 3 (very high) vulnerability.

3. Results

3.1. Cooling Effects of Total Green Space on Land Surface Temperature

Fig. 2 illustrates the relationship between TGS fraction and LST across four seasons, separated into urban pixels (LCZ 1–9; Fig. 2a) and natural pixels (LCZ A–G; Fig. 2b). Grid cells were grouped into 5% TGS intervals, and LST distributions within each group were summarized by the median and interquartile range.

Across all seasons, higher TGS fractions were associated with lower LSTs. The strongest effect occurred in summer (Fig. 2d), where urban pixels with 0% TGS had a median LST of 30.3°C, compared with 27.7°C for pixels with 80% TGS (2.6°C difference). Spring (Fig. 2c) and fall (Fig. 2e) showed differences of 1.6°C and 1.2°C, respectively, while winter (Fig. 2f) showed only a 0.4°C difference. In winter, urban pixels with TGS ≥40% were slightly cooler than natural LCZ pixels, reversing the typical urban–rural contrast. A nonlinear pattern was evident in all seasons: cooling benefits were substantial up to about 40% TGS and then diminished. In natural LCZs, the relationship remained nearly linear, with increasing vegetation cover consistently lowering LST.

3.2. Variability of Vegetation-Temperature Relationships across LCZs

Fig. 3 and 4 examine whether vegetation–temperature relationships differ by LCZ. Fig. 3 shows LST distributions for LCZ 1–6, 8, and 9, separated into TGS fraction groups (0–20%, 20–40%, 40–60%, and 60–80%). In most LCZs, the distributions shifted toward lower LSTs with higher TGS fractions. The effect was strongest in LCZ 1 (compact high-rise), with reductions in median LST and fewer extremely hot pixels. LCZ 2 and 3 (compact mid- and low-rise) showed similar but more modest changes than LCZ 1. In open LCZs (4–6), the contrast between the lowest vegetation group (0–20% TGS) and higher groups was more apparent than the differences among the higher categories. LCZ 4 and 5 (open high- and mid-rise) showed broadly similar distributions, but LCZ 4 grids tended to shift toward slightly cooler values. This pattern resembles that of LCZ 1, suggesting that the combined effect of building shading and vegetation is more effective in LCZ 4 than in LCZ 5.

Vegetation also reduced the spread of LST values. In high-TGS groups, the distribution was narrower, with fewer pixels exceeding 32°C. Fig. 4 further shows seasonal median LSTs by LCZ and TGS group. In summer, LCZ 1 cooled by about 1.0°C

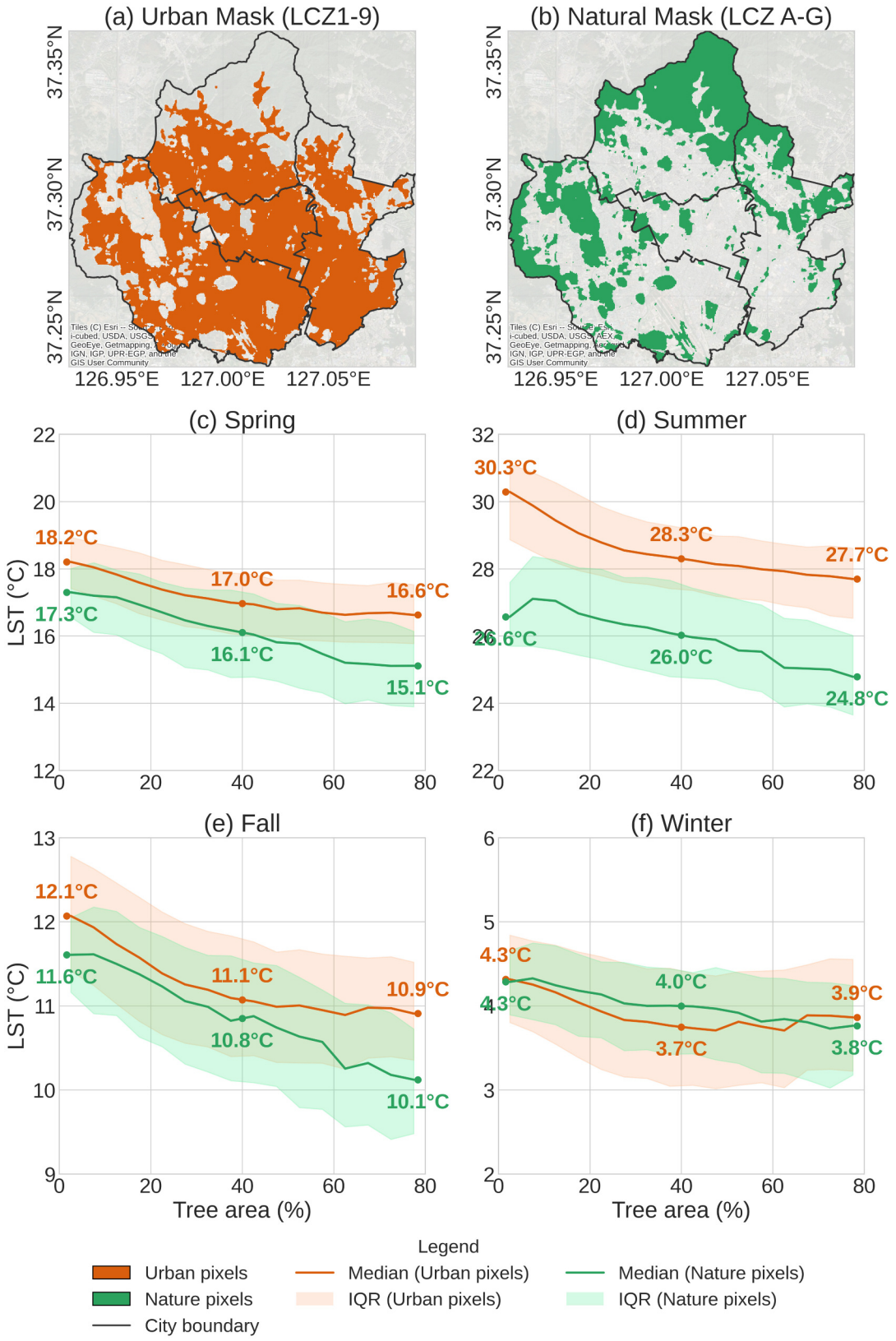

Fig. 2. Seasonal relationship between total green space (TGS) fraction and land surface temperature (LST). (a) Urban pixels (LCZ 1–9) and (b) natural pixels (LCZ A–G) masks for Suwon. (c–f) Median (solid line) and interquartile range (shaded band) of LST across 5% TGS intervals for spring, summer, fall, and winter, respectively.

https://doi.org/10.7780/kjrs.2025.41.5.11

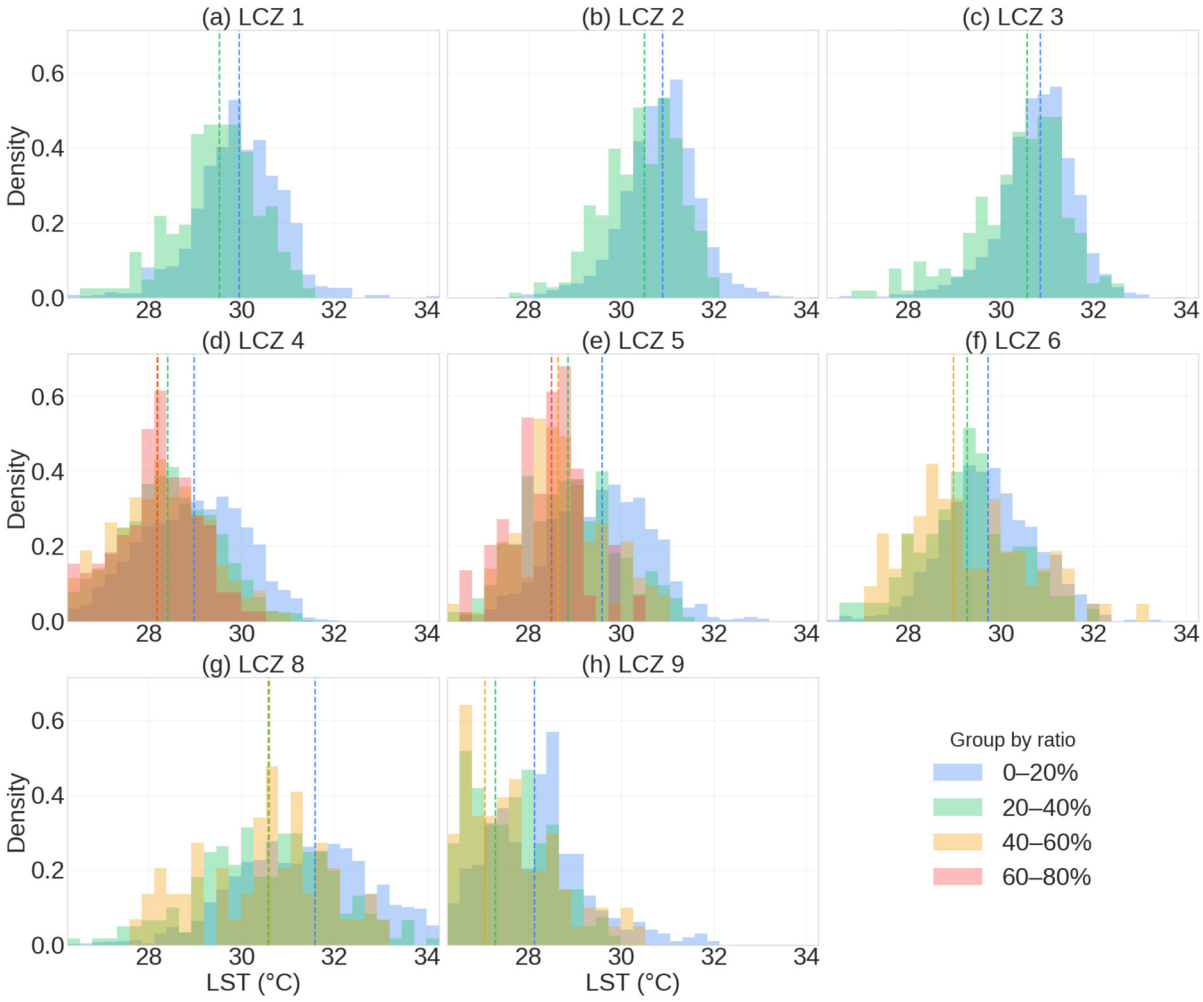

Fig. 3. Summer LST distributions stratified by LCZ class (LCZ 1–6, 8, and 9) and total green space (TGS) fraction groups (0–20%, 20–40%, 40–60%, and 60–80%).

between the lowest and highest TGS groups, while LCZ 2 cooled by 0.7°C, LCZ 3 cooled by 0.9°C, LCZ 4 cooled by 0.9°C, LCZ 5 cooled by 1°C, and LCZ 6 cooled by 0.5°C. These patterns demonstrate that increasing urban tree cover consistently reduces median LST across a range of morphological types, though the absolute magnitude of cooling may vary. Seasonal differences were largest in summer, moderate in spring and fall, and minimal in winter (<0.2°C).

3.3. Spatial Inequity of Green Space Provision across Neighborhoods

Fig. 5 summarizes the dong-level green space composition across Suwon. Peripheral neighborhoods near hillslopes retained large FC shares, while TGS ratios declined sharply in central districts, where vegetation consisted almost entirely of UTC. For example, Yeonmu-dong and Pajang-dong, both situated at the northern edge, had the highest TGS ratios (>70%), dominated by FC, whereas Seryu 3(sam)-dong, Ji-dong, and Yeonghwa-dong in the urban core had extremely limited TGS (<10%), almost entirely from UTC. UTC fractions range from 7 to 31% across dongs, typically lower than FC fractions (0–72%) in peripheral areas. However, UTC was the only vegetation source in central areas lacking forest.

Beyond the absolute share of forest and urban tree canopy, the adequacy of green space must also be evaluated relative to population distribution. Peripheral neighborhoods maintain high TGS ratios (Fig. 6a) and relatively low population densities (Fig. 6b), while many central districts have both lower TGS ratios and higher population densities. The lack of green space in these urban cores becomes even more pronounced when evaluated on a per capita basis (Fig. 6c), with ten neighborhoods falling below the WHO minimum standard of 9 m^2 per person. Fig. 6d shows

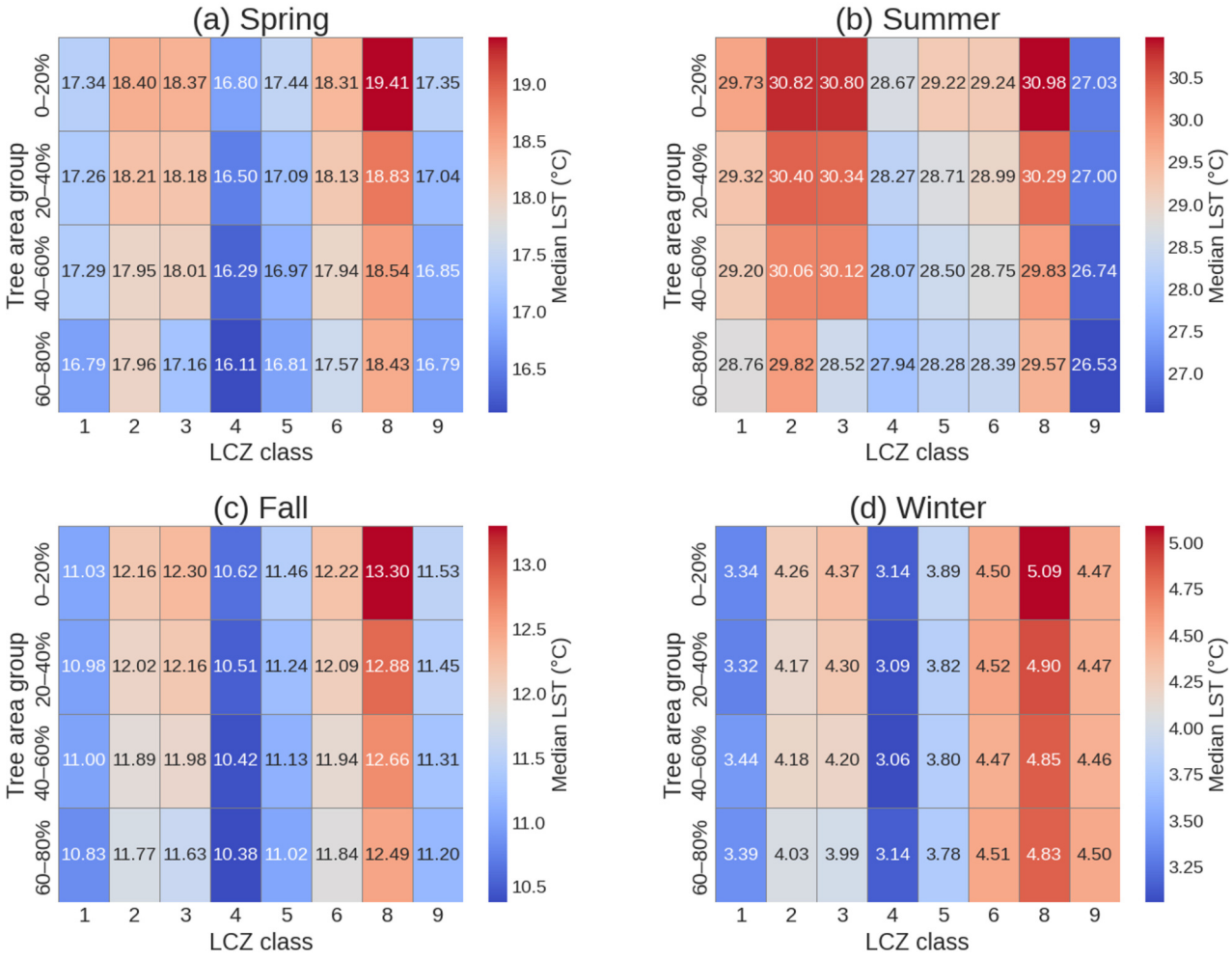

Fig. 4. Seasonal heatmaps of median LST by LCZ class and TGS fraction group.

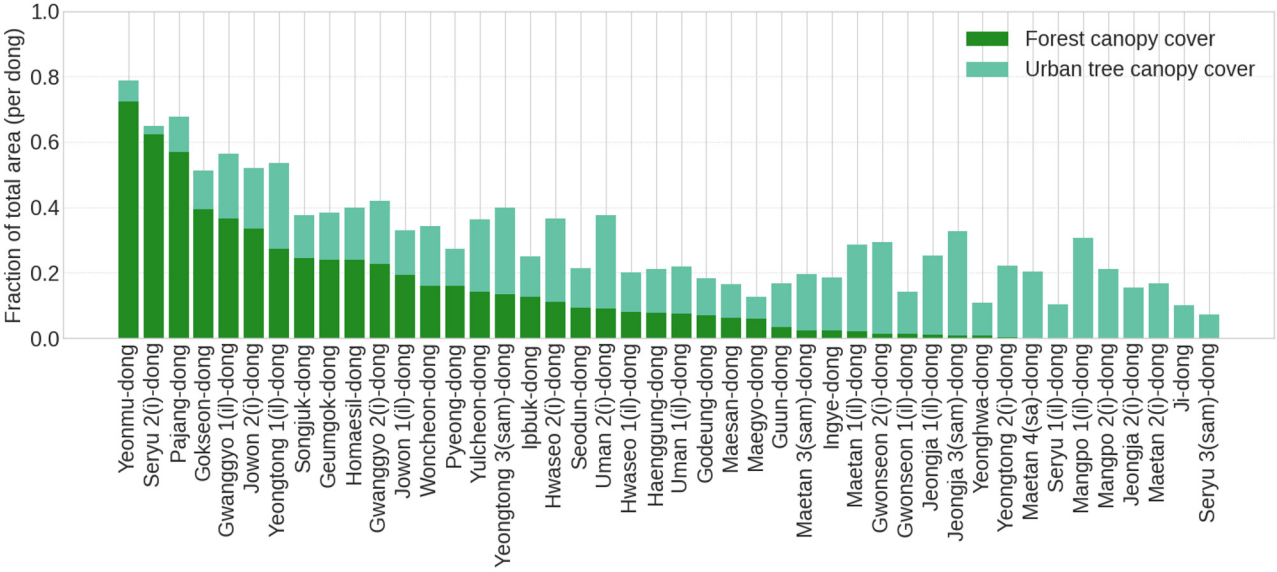

Fig. 5. Dong-level green space composition sorted by total green space ratio; bars split into forest canopy (FC) and urban tree canopy (UTC). Peripheral, hill-adjacent dongs concentrate FC, whereas most central districts depend primarily on UTC for greening.

https://doi.org/10.7780/kjrs.2025.41.5.11

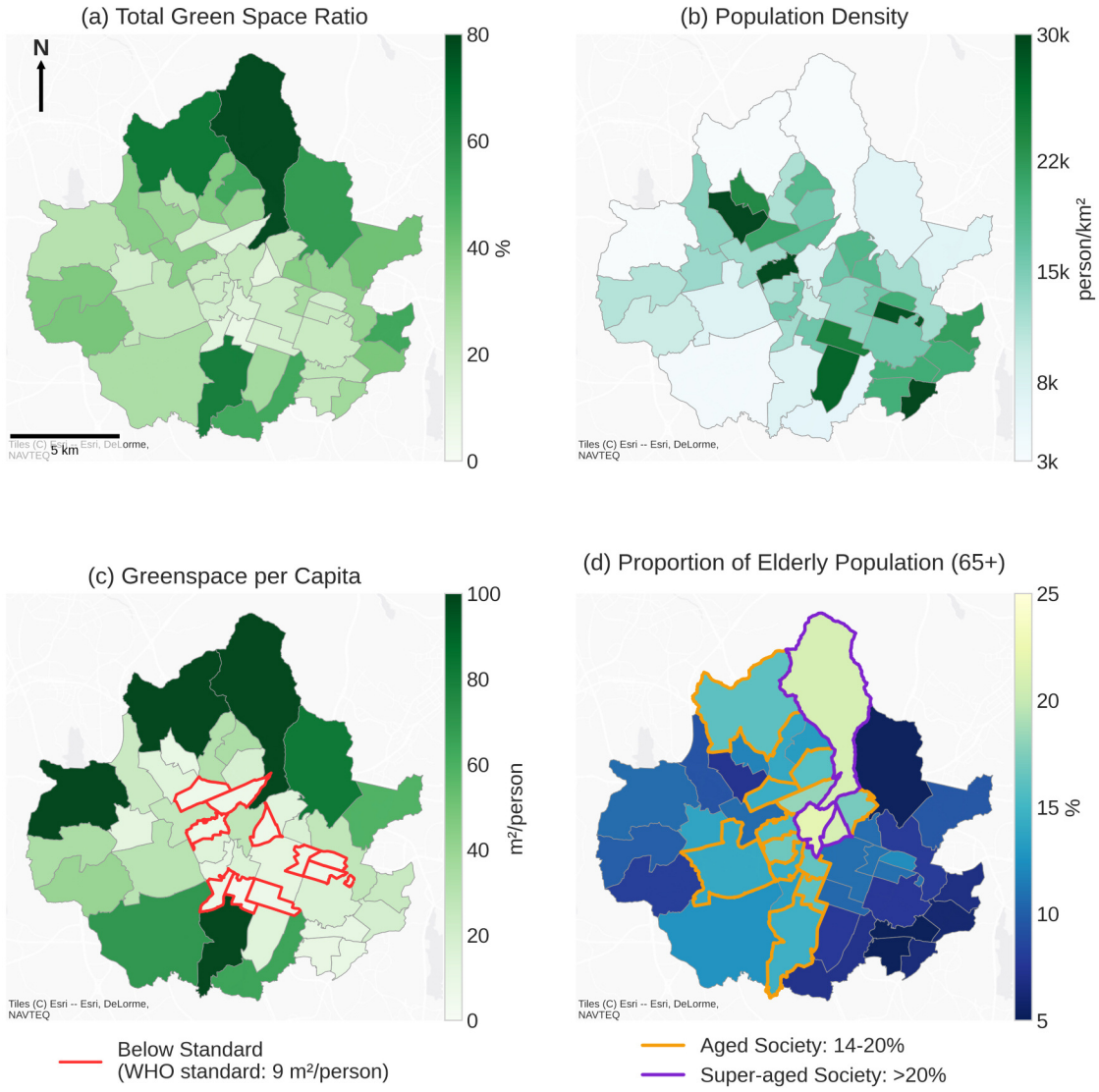

Fig. 6. Choropleths of (a) TGS ratio, (b) population density, (c) greenspace per capita (red outlines: WHO <9 m²/person), and (d) elderly population (orange/purple outlines: ≥14%/≥20%).

the share of elderly residents (65+) across neighborhoods, with orange outlines marking "aged" societies (≥14%) and purple outlines marking "super-aged" societies (≥20%) according to the UN definition. Five of these aged and super-aged districts overlap with areas of limited green space provisions, indicating that elderly populations are disproportionately concentrated in vegetation-scarce neighborhoods.

3.4. Linking Green Space Inequity to Vulnerability under Urban Heat

Fig. 7(a) plots TGS against summer mean LST at the dong level, with colors denoting elderly population categories. Districts with low TGS generally had high LSTs. Many of these hot, vegetation-scarce neighborhoods were also classified as aged (≥14%) or super-aged (≥20%). To identify where these vulnerabilities cluster, we developed a composite index with three criteria: (i) greenspace per capita below 9 m² per person, (ii) elderly population share above 14%, and (iii) summer mean LST in the upper quartile. Districts satisfying all three were scored as 3 ("very high" vulnerability). Fig. 7(b) highlights three central neighborhoods—Seryu 3(sam)-dong, Ji-dong, and Yeonghwa-dong—as having very high vulnerability. Districts meeting two criteria were scored as 2 (high vulnerability) with three combinations. First, Maetan 4(sa)-dong, Gwonseon 1(il)-dong, and Maetan 2(i)-dong exhibit both greenspace scarcity and high summer LSTs, pointing to strong environmental exposure. Second, Seryu 2(i)-dong, Maesan-dong,

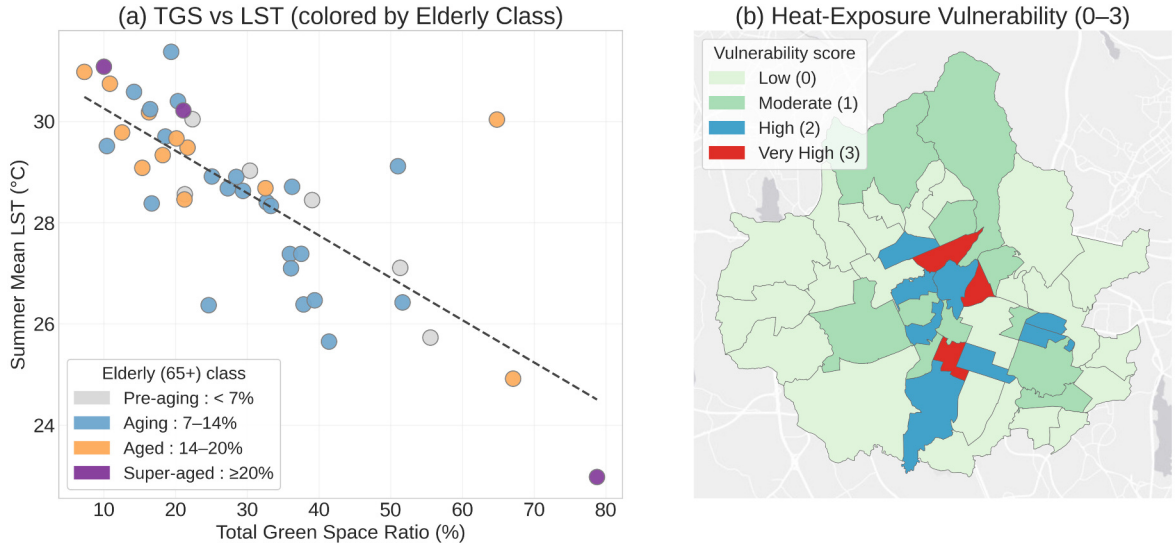

Fig. 7. Linking green space to heat vulnerability across Suwon. (a) Relationship between total green space (TGS) ratio and summer mean land surface temperature (LST) at the dong level, with marker colors indicating elderly population classes following the UN definition (Pre-aging: <7%, aging: 7–14%, aged: 14–20%, super-aged: ≥20%). (b) Composite vulnerability index (0–3) integrating three criteria: greenspace per capita below the WHO minimum standard of 9 m^2 per person, elderly population ≥14%, and LST values in the upper quartile of the citywide distribution.

and Haenggung-dong combine elevated heat with an aged or super-aged population, highlighting areas where demographic sensitivity and heat exposure converge. Third, Jeongja 2(i)-dong and Hwaseo 1(il)-dong are characterized by limited green spaces and high elderly shares, underscoring neighborhoods where social vulnerability coincides with insufficient ecological buffers.

4. Discussion

This study is the first to integrate high-resolution urban vegetation mapping with the LCZ framework to examine vegetation–temperature relationships within a single city. By combining detailed canopy data with LCZ classification, we assessed vegetation's cooling effects both citywide and within distinct urban morphologies, moving beyond conventional citywide analyses that often overlook intra-urban morphological variability.

The vegetation–temperature relationship in Suwon exhibited two distinct behaviors depending on the vegetation context. FC pixels located in natural LCZs showed an almost linear cooling trend, with LST decreasing steadily as vegetation fraction increased. In contrast, UTC pixels within built LCZs exhibited a pronounced nonlinear response—cooling intensified rapidly up to about 40% canopy cover and then plateaued, indicating diminishing marginal returns under dense urban morphology. This nonlinear saturation was also reported by Zhan et al. (2024), who observed nonlinear trends in cooling efficiency across 440 cities globally.

However, their assessment was conducted at the city-aggregated scale, averaging vegetation and temperature conditions across entire metropolitan areas. In contrast, our study resolves this relationship at the intra-urban pixel level by incorporating the 0.25 m tree-canopy map and LCZ-based morphological context. This finer-scale perspective reveals that the same nonlinear cooling behavior persists even within a single city, suggesting that the diminishing marginal cooling benefits of vegetation may represent a scale-invariant feature of urban thermal environments.

The contrasting cooling patterns between natural and urban LCZs highlight how vegetation–temperature relationships are moderated by built morphology. In compact high-rise zones (LCZ 1), vegetation produced the strongest overall cooling despite limited spatial extent. This likely reflects a high cooling efficiency per unit canopy area, a phenomenon that has also been demonstrated in recent studies (Cai et al., 2025). In contrast, in open low-rise LCZs, the same canopy fraction provides broader but less intense cooling, as heat dissipation occurs more efficiently under open urban geometries with greater sky exposure (Chen et al., 2023).

Beyond the physical cooling effects, our analysis highlights the social dimension of thermal inequity. The unequal distribution of vegetation across Suwon—dense forest canopies concentrated in the periphery and sparse urban trees dominating the core—reflects long-standing land-use legacies and urban development trajectories. Central districts with higher population density

https://doi.org/10.7780/kjrs.2025.41.5.11

and older building stock have limited space and institutional flexibility for green expansion, whereas peripheral zones have retained remnant natural cover. In addition, large newly developed residential districts have emerged in these peripheral areas, where urban planning regulations mandate minimum green-space ratios and roadside tree planting, further reinforcing the vegetation contrast between old central neighborhoods and newly built suburbs. Consequently, these spatial disparities overlap with demographic vulnerabilities, leaving elderly populations in under-greened areas more exposed to higher thermal risk. This is a pattern consistent with global evidence linking social disadvantage and environmental risk (Harlan et al., 2006; Zhou et al., 2021; McNeil et al., 2025).

4.1. Uncertainties and Limitations

First, although the Landsat TIRS Band 10 product is distributed at 30 m resolution, its native instantaneous field of view is approximately 100 m. Therefore, each 30 m pixel effectively represents the averaged thermal emission from a broader area, introducing scale-induced averaging rather than true sub-pixel detail. While we mitigated this by incorporating a 0.25 m canopy map to estimate the vegetation fraction within each pixel, the retrieved LST still reflects an area-mean temperature, rather than the actual surface temperature of individual materials.

Second, the analysis relied on a limited number of clear-sky Landsat 8 scenes (2019–2021). Vegetation–temperature interactions may vary over shorter time scales due to phenology, soil moisture, and atmospheric humidity. Higher temporal-frequency observations—such as ECOSTRESS thermal imagery or dense in-situ sensor networks—would better capture transient heat dynamics.

Finally, the vulnerability index developed here is descriptive rather than predictive. It identifies priority areas for intervention but does not directly quantify health outcomes. Validation against heat-related morbidity or mortality data at the dong scale was not feasible because such data are not publicly available in South Korea.

4.2. Policy Relevance

Our findings provide actionable insights for urban planners seeking to mitigate urban heat while promoting equitable green distribution. The quantified vegetation–temperature relationships across LCZ types offer empirical benchmarks for setting morphology-specific greening targets. The results demonstrate that the efficiency of urban greening is governed by the three-dimensional built form rather than vegetation quantity alone, suggesting that greening strategies should be tailored to local morphological context.

Moreover, the spatial overlap between high heat exposure, limited vegetation, and a high proportion of elderly residents highlights priority areas for targeted intervention. Municipal planners can adopt this integrated framework to identify neighborhoods where small-scale greening actions would yield the greatest combined thermal and social benefits. In practice, such morphology- and equity-informed guidelines can support the development of quantitative greening standards under municipal climate adaptation plans and urban forest strategies.

4.3. Future Directions

Future research should extend this framework in both temporal and thematic dimensions. First, incorporating long-term Landsat L2 ST products would allow examination of how vegetation–temperature relationships evolve under changing phenology or climate conditions in Suwon. Second, coupling LST with air temperature and humidity data will enable evaluation of human-perceived thermal comfort, not just surface heat. Third, integrating health outcome and exposure datasets will facilitate quantitative validation of vulnerability estimates, bridging environmental exposure with public-health risk. Finally, expanding this high-resolution, fraction-dependent vegetation–LST framework to multiple cities across different climatic and morphological contexts will enable comparative analyses and evidence-based design of equitable, climate-resilient urban greening policies.

5. Conclusions

By integrating a 0.25 m urban vegetation map with the LCZ framework and 30 m Landsat 8-derived LST, this study revealed how vegetation fraction and urban morphology jointly regulate surface temperature within a city. The results demonstrate two distinct behaviors: a near-linear cooling trend in FC and a nonlinear response in UTC, where cooling intensified up to about 40% canopy cover and then plateaued. This indicates that vegetation's cooling efficiency is governed not only by canopy abundance but also by three-dimensional urban form. The strongest per-area cooling was observed in compact high-rise districts, underscoring the importance of even limited greening in dense urban cores. At the same time, vegetation scarcity and demographic vulnerability were spatially coupled in older central districts, highlighting the need to integrate thermal mitigation and social equity. Together, these findings provide an empirical

basis for morphology-specific, evidence-driven greening policies, guiding urban planners toward more effective and equitable climate-resilient city design.

Author Contributions

Conceptualization: Lee YS, Im JH; Data curation: Lee YS, Jegal S, Lee SW, Son BK; Formal analysis: Lee YS, Jegal S; Investigation: Lee YS, Jegal S, Lee SW, Son BK; Methodology: Lee YS; Resources: Lee SW, Son BK, Im JH; Funding acquisition, Supervision: Im JH; Writing–original draft: Lee YS, Lee SW; Writing–review & editing: All authors.

Conflicts of Interest

No potential conflict of interest relevant to this article was reported.

Funding

This research was supported by Development of Comprehensive Land Management Technology Using Satellite Image Information Big Data Project funded by the Ministry of Land, Infrastructure, and Transport of the Korean government (RS-2022-00155763), Basic Science Research Program through the National Research Foundation of Korea (NRF) funded by the Ministry of Education (RS-2024-00409948) and NRF grant funded by the Ministry of Science and Information and Communication Technology (NRF-2021R1A2C2008561).

Data Availability Statement

The high-resolution land cover dataset used in this study was produced by Son et al. (2021) and is available from the corresponding author upon reasonable request. Landsat 8 data are openly available from the USGS EarthExplorer portal (https://earthexplorer.usgs.gov/). The LCZ map was developed in Lee et al. (2023b) and is available from the authors upon request. Socioeconomic and demographic statistics for Suwon were obtained from the Suwon Statistical Yearbook, which is publicly accessible at https://data.suwon.go.kr/portal/main

Acknowledgments

None.

Supplementary Materials

Fig. S1. Data gaps in Landsat-8 L2 Surface Temperature (ST) over Suwon caused by missing ASTER GED emissivity

Table S1. Pixel-wise comparison between Landsat-8 L2 ST and the single-channel L1 Band-10 LST retrieval

Table S2. Comparison of in-situ LST, single-channel L1 LST, and Landsat-8 L2 ST, time-matched to Landsat overpass (~10:30 KST)

Table S3. Sensitivity of seasonal LST composites

References

Alonzo, M., Ibsen, P. C., and Locke, D. H., 2025. Urban trees and cooling: A review of the recent literature (2018 to 2024). *Arboriculture & Urban Forestry, 51*(5), 420–444. https://doi.org/10.48044/jauf.2025.023

Cai, M., Li, M., and Liu, H., 2025. Optimizing cooling efficiency of urban greenspaces across local climate zones in Wuhan, China. *Urban Forestry & Urban Greening, 105*, 128691. https://doi.org/10.1016/j.ufug.2025.128691

Chakraborty, T. C., Lee, X., Ermida, S., and Zhan, W., 2021. On the land emissivity assumption and Landsat-derived surface urban heat islands: A global analysis. *Remote Sensing of Environment, 265*, 112682. https://doi.org/10.1016/j.rse.2021.112682

Chen, C., Bagan, H., and Yoshida, T., 2023. Multiscale mapping of local climate zones in Tokyo using airborne LiDAR data, GIS vectors, and Sentinel-2 imagery. *GIScience & Remote Sensing, 60*(1), 2209970. https://doi.org/10.1080/15481603.2023.2209970

Crawford, C. J., Roy, D. P., Arab, S., Barnes, C., Vermote, E., Hulley, G., et al., 2023. The 50-year Landsat collection 2 archive. *Science of Remote Sensing, 8*, 100103. https://doi.org/10.1016/j.srs.2023.100103

Derickson, K., Walker, R., Hamann, M., Anderson, P., Adegun, O. B., Castillo-Castillo, A., et al., 2024. The intersection of justice and urban greening: Future directions and opportunities for research and practice. *Urban Forestry & Urban Greening, 95*, 128279. https://doi.org/10.1016/j.ufug.2024.128279

Du, J., Jiang, S., Cui, B., Wu, G., and Liu, H., 2022. Observation-based evaluation of local climate effect of terrestrial vegetation in temperate zones. *Journal of Geophysical Research: Atmospheres, 127*(12), e2021JD036313. https://

doi.org/10.1029/2021JD036313

Falchetta, G., De Cian, E., Sue Wing, I., and Carr, D., 2024. Global projections of heat exposure of older adults. *Nature Communications, 15*(1), 3678. https://doi.org/10.1038/s41467-024-47197-5

Gao, S., Chen, Y., Chen, D., He, B., Gong, A., Hou, P., et al., 2024. Urbanization-induced warming amplifies population exposure to compound heatwaves but narrows exposure inequality between global North and South cities. *npj Climate and Atmospheric Science, 7*, 154. https://doi.org/10.1038/s41612-024-00708-z

Gillerot, L., Landuyt, D., De Frenne, P., Muys, B., and Verheyen, K., 2024. Urban tree canopies drive human heat stress mitigation. *Urban Forestry & Urban Greening, 92*, 128192. http://doi.org/10.1016/j.ufug.2023.128192

Guo, J., Ren, H., Zheng, Y., Lu, S., and Dong, J., 2020. Evaluation of land surface temperature retrieval from Landsat 8/TIRS images before and after stray light correction using the SURFRAD dataset. *Remote Sensing, 12*(6), 1023. https://doi.org/10.3390/rs12061023

Harlan, S. L., Brazel, A. J., Prashad, L., Stefanov, W. L., and Larsen, L., 2006. Neighborhood microclimates and vulnerability to heat stress. *Social Science & Medicine, 63*(11), 2847–2863. https://doi.org/10.1016/j.socscimed.2006.07.030

Heo, S., Nori-Sarma, A., Kim, S., Lee, J. T., and Bell, M. L., 2021. Do persons with low socioeconomic status have less access to greenspace? Application of accessibility index to urban parks in Seoul, South Korea. *Environmental Research Letters, 16*(8), 084027. https://doi.org/10.1088/1748-9326/ac12f1

Independent Evaluation Group, 2019. World Bank Support to Aging Countries (Approach Paper). Available online: http://documents.worldbank.org/curated/en/870611561130594816 (assessed on Sept. 30, 2025).

Jeevalakshmi, D., Reddy, S. N., and Manikiam, B., 2017. Land surface temperature retrieval from Lansat data using emissivity estimation. *International Journal of Applied Engineering Research, 12*(20), 9679–9687.

Jung, M. C., Dyson, K., and Alberti, M., 2021. Urban landscape heterogeneity influences the relationship between tree canopy and land surface temperature. *Urban Forestry & Urban Greening, 57*, 126930. https://doi.org/10.1016/j.ufug.2020.126930

Kim, J., and Kang, W., 2022. Assessing green roof contributions to tree canopy ecosystem services and connectivity in a highly urbanized area. *Land, 11*(8), 1281. https://doi.org/10.3390/land11081281

Kofel, D., Bourgeois, I., Paganini, R., Pulfer, A., Grossiord, C., and Schmale, J., 2024. Quantifying the impact of urban trees on air quality in Geneva, Switzerland. *Urban Forestry & Urban Greening, 101*, 128513. https://doi.org/10.1016/j.ufug.2024.128513

Koppe, C., Kovats, S., Jendritzky, G., Menne, B., Baumüller, J., and Bitan, A., et al., 2004. Heat-waves: Risks and responses. In: *Health and Global Environmental Change* (Series, No. 2). World Health Organization Regional Office for Europe. https://iris.who.int/server/api/core/bitstreams/98e898c9-81f6-4131-8178-58983f15737b/content

Kuchelmeister, G., 1998. *Urban forestry in the Asia-Pacific region: Status and prospects*. Forestry Policy and Planning Division. https://books.google.co.kr/books?id=ENYsAQAAMAAJ

Lee, J.-Y., Jung, S.-W., and Hong, S.-H., 2023a. Mapping lava flow from the Kilauea eruption of 2018 in the east rift zone using space-based synthetic aperture radar. *GIScience & Remote Sensing, 60*(1), 2176275. https://doi.org/10.1080/15481603.2023.2176275

Lee, Y., Lee, S., Im, J., and Yoo, C., 2021. Analysis of surface urban heat island and land surface temperature using deep learning based local climate zone classification: A case study of Suwon and Daegu, Korea. *Korean Journal of Remote Sensing, 37*(5–3), 1447–1460. https://doi.org/10.7780/kjrs.2021.37.5.3.9

Lee, Y., Son, B., Im, J., Zhen, Z., and Quackenbush, L. J., 2024. Two-step carbon storage estimation in urban human settlements using airborne LiDAR and Sentinel-2 data based on machine learning. *Urban Forestry & Urban Greening, 94*, 128239. https://doi.org/10.1016/j.ufug.2024.128239

Lee, S., Yoo, C., Im, J., Cho, D., Lee, Y., and Bae, D., 2023b. A hybrid machine learning approach to investigate the changing urban thermal environment by dynamic land cover transformation: A case study of Suwon, Republic of Korea. *International Journal of Applied Earth Observation and Geoinformation, 122*, 103408. https://doi.org/10.1016/j.jag.2023.103408

Li, W., and Li, C., 2025. Racial inequalities in urban tree canopy exposure across major cities in the United States. *Urban Forestry & Urban Greening, 112*, 128974. https://doi.org/10.1016/j.ufug.2025.128974

Liu, X., Liang, S., Ma, H., Li, B., Zhang, Y., Li, Y., et al., 2024. Landsat-observed changes in forest cover and attribution

analysis over Northern China from 1996–2020. *GIScience & Remote Sensing, 61*(1), 2300214. https://doi.org/10.1080/15481603.2023.2300214

McNeil, W. H., Porzio, J., Tong, F., Harley, R. A., Auffhammer, M., and Scown, C. D., 2025. Impact of truck electrification on air pollution disparities in the United States. *Nature Sustainability, 8*, 276–286. https://doi.org/10.1038/s41893-025-01515-x

Na, N., Lou, D., Xu, D., Ni, X., Liu, Y., and Wang, H., 2024. Measuring the cooling effects of green cover on urban heat island effects using Landsat satellite imagery. *International Journal of Digital Earth, 17*(1), 2358867. https://doi.org/10.1080/17538947.2024.2358867

Pourpeikari Heris, M., Bagstad, K. J., Troy, A. R., and O'Neil-Dunne, J. P. M., 2022. Assessing the accuracy and potential for improvement of the national land cover database's tree canopy cover dataset in urban areas of the conterminous United States. *Remote Sensing, 14*(5), 1219. https://doi.org/10.3390/rs14051219

Shi, K., Wu, Y., Liu, S., Chen, Z., Huang, C., and Cui, Y., 2023. Mapping and evaluating global urban entities (2000–2020): A novel perspective to delineate urban entities based on consistent nighttime light data. *GIScience & Remote Sensing, 60*(1), 2161199. https://doi.org/10.1080/15481603.2022.2161199

Sobrino, J. A., Jiménez-Muñoz, J. C., and Paolini, L., 2004. Land surface temperature retrieval from Landsat TM 5. *Remote Sensing of Environment, 90*(4), 434–440. https://doi.org/10.1016/j.rse.2004.02.003

Somvanshi, A., Schulze, J., and Talebsafa, S., 2025. Urban Heat Typologies: Impact of heatwaves on urban built environment and heat stress risk to the elderly in Darmstadt, Germany. *City and Environment Interactions, 28*, 100231. https://doi.org/10.1016/j.cacint.2025.100231

Son, B., Lee, Y., and Im, J., 2021. Classification of urban green space using airborne LiDAR and RGB ortho imagery based on deep learning. *Journal of the Korean Association of Geographic Information Studies, 24*(3), 83–98. https://doi.org/10.11108/kagis.2021.24.3.083

Stewart, I. D., and Oke, T. R., 2012. Local climate zones for urban temperature studies. *Bulletin of the American Meteorological Society, 93*(12), 1879–1900. https://doi.org/10.1175/BAMS-D-11-00019.1

Sun, C., Li, J., Liu, Y., Pan, T., Shi, K., and Cai, X., 2024. Synthesizing Landsat images using time series model-fitting methods for China's coastal areas against sparse and irregular observations. *GIScience & Remote Sensing, 61*(1), 2421574. https://doi.org/10.1080/15481603.2024.2421574

Suwon Council for Sustainable Development, 2021. *Suwon SDGs Action Report in line with UN 2030 Agenda for sustainable development: The implementation of the UN sustainable development goals in Suwon 2020*. Suwon Council for Sustainable Development. https://www.iges.or.jp/sites/default/files/inline-files/2021%20-%20Suwon.pdf

United States Geological Survey, 2025a. Landsat Collection 2 Known Issues. Available online: https://www.usgs.gov/landsat-missions/landsat-collection-2-known-issues (Assessed on Oct. 18, 2025).

United States Geological Survey, 2025b. Landsat Level-1 Processing Details. Available online: https://www.usgs.gov/landsat-missions/landsat-level-1-processing-details (Assessed on Oct. 18, 2025).

Valor, E., and Caselles, V., 1996. Mapping land surface emissivity from NDVI: Application to European, African, and South American areas. *Remote Sensing of Environment, 57*(3), 167–184. https://doi.org/10.1016/0034-4257(96)00039-9

Wang, X., Scott, C. E., and Dallimer, M., 2023. High summer land surface temperatures in a temperate city are mitigated by tree canopy cover. *Urban Climate, 51*, 101606. https://doi.org/10.1016/j.uclim.2023.101606

Wu, C. C., O'Keefe, J., Ding, Y., and Sullivan, W. C., 2024. Biodiversity of urban green spaces and human health: A systematic review of recent research. *Frontiers in Ecology and Evolution, 12*, 1467568. https://doi.org/10.3389/fevo.2024.1467568

Xie, Q., Wu, Y., Zhou, Z., and Wang, Z., 2018. Remote sensing study of the impact of vegetation on thermal environment in different contexts. *IOP Conference Series: Earth and Environmental Science, 121*, 022009. https://doi.org/10.1088/1755-1315/121/2/022009

Yin, H., Chen, C., Dong, Q., Zhang, P., Chen, Q., and Zhu, L., 2022. Analysis of spatial heterogeneity and influencing factors of ecological environment quality in China's North–South Transitional Zone. *International Journal of Environmental Research and Public Health, 19*(4), 2236. https://doi.org/10.3390/ijerph19042236

Yin, Y., Li, S., Xing, X., Zhou, X., Kang, Y., Hu, Q., et al., 2024. Cooling benefits of urban tree canopy: A systematic review. *Sustainability, 16*(12), 4955. https://doi.org/10.3390/su16124955

Yoo, C., Lee, Y., Cho, D., Im, J., and Han, D., 2020. Improving local climate zone classification using incomplete building data and Sentinel 2 images based on convolutional neural networks. *Remote Sensing, 12*(21), 3552. https://doi.org/10.3390/rs12213552

Zhan, W., Wang, C., Wang, S., Li, L., Ji, Y., Du, H., et al., 2024. Fraction-dependent variations in cooling efficiency of urban trees across global cities. *ISPRS Journal of Photogrammetry and Remote Sensing, 216*, 229–239. https://doi.org/10.1016/j.isprsjprs.2024.07.026

Zhou, W., Huang, G., Pickett, S. T. A., Wang, J., Cadenasso, M. L., McPhearson, T., et al., 2021. Urban tree canopy has greater cooling effects in socially vulnerable communities in the US. *One Earth, 4*(12), 1764–1775. https://doi.org/10.1016/j.oneear.2021.11.010